the current controller. Many points in Fig. 13 denote corresponding speed–torque values under various conditions suggested in Tables II and III, in which cross points (×) imply that the DuPG could not achieve the desired velocity over the combined characteristics graph of the DuPG. The square points (□) imply that the two motors spent a large current (more than $0.4[A]$) for achieving the desired speed, and the circle points (◯) imply that the DuPG could satisfy the desired velocity within the required current condition $0.4[A]$. When the current controller was not utilized, many circle points (◯) in Fig. 13(a) were located outside of combined characteristics graph. However, when the current controller was used for reducing the current difference between the two motors, we could confirm from Fig. 13(b) that ◯ points were moved into the 0.4[A] region (into the continuous operation region) and some □ were changed into ◯. Moreover, the number of square points (□) over 0.4[A] were reduced when using the current controller. Since the DuPG system using the suggested current control method could operate in low current and continuous operation region, it could improve energy efficiency. The operation region can be classified as high-speed with low-torque, low-speed with high-torque, and low-speed with low-torque (the operation regions of motor 1 and motor 2 are overlapped). When the mobile robot operates at a low-speed with low-torque with two overlapped motors, the two motors spend small currents. Thus, if we select the parameters of the DuPG in Table I for purposes with which mobile robots are usually controlled, low-speed with low-torque, the robot can achieve high energy efficiency due to the consumption of small currents. Through the experiment results, we could see that the suggested DuPG generates the combined characteristics graphs according to the different purposes.

IV. Concluding Remarks

This paper has suggested a novel actuator system using a planetary gear (DuPG) and two motors for mobile robot applications, which was able to generate high speed or high torque according to environmental or driving conditions. Also, the proposed actuator system not only extends the speed/torque operation region but also operates with energy efficiency by reducing the required currents. In this paper, two types of actuator systems have been verified through simulations and experiments; Type 1 for replacing a big motor with two small motors and Type 2 for operating like the automatic gear-transmission of an automobile. Moreover, the prototype of the DuPG can easily be fabricated with a small gear box including the planetary and worm gears, ultimately, for compact actuator systems and small-sized mobile robot applications.

References

[1] J. Kim and S. B. Choi, "Design and modeling of a clutch actuator system with self-energizing mechanism," *IEEE/ASME Trans. Mechatronics*, vol. 15, no. 5, pp. 1–14, 2010.

[2] T. Lam, H. Qian, and Y Xu, "Omnidirectional steering interface and control for a four-wheel independent steering vehicle," *IEEE/ASME Trans. on Mechatronics*, [Online]. Available: 10.1109/TMECH.2009.2024938, 2010.

[3] L. Glielmo, L. Iannelli, V. Vacca, and F. Vasca, "Gearshift control for automated manual transmission," *IEEE/ASME Trans. Mechatronics*, vol. 11, no. 1, pp. 17–26, 2006.

[4] H. Lee, C. Lee, S. Kim, and Y. Choi, "New actuator system using movable pulley for bio-mimetic system and wearable robot applications," in *Proc. IEEE Int. Conf. Robot. Autom.*, 2010, pp. 2183–2188.

[5] B.-S. Kim, J.-B. Song, and J.-J. Park, "A serial-type dual actuator unit with planetary gear train: Basic design and applications," *IEEE/ASME Trans. Mechatronics*, vol. 15, no. 1, pp. 108–116, 2010.

[6] B.-S. Kim, J.-J. Park, and J.-B. Song, "Double actuator unit with planetary gear train for a safe manipulator," in *Proc. IEEE Int. Conf. Robot. Autom.*, 2007, pp. 1146–1151.

[7] J. Morrell and J. Salisbury, "In pursuit of dynamic range: Using parallel coupled actuators to overcome hardware limitations," in *Proc. 4th Int. Symp. Exp. Robot. IV*, London, U.K., 1995, pp. 263–273.

[8] M. Zinn, O. Khatib, and B. Roth, "A new actuation approach for human friendly robot design," in *Proc. IEEE Int. Conf. Robot. Autom., (ICRA)*, New Orleans, LA, Apr. 26–May 1, 2004, pp. 249–254.

[9] T.-J. Yeh and F.-K. Wu, "Modeling and robust control of worm-gear driven systems," *Simulat. Modell. Practice Theory*, vol. 17, no. 5, pp. 267–777, 2009.

[10] D. May, S. Jayasuriya, and B. Mooring, "Modeling and control of a manipulator joint driven through a worm gear transmission," *J. Vibrat. Control*, vol. 6, no. 1, pp. 85–111, 2000.

An Artificial Muscle Ring Oscillator

Benjamin Marc O'Brien and Iain Alexander Anderson

***Abstract*—Dielectric elastomer artificial muscles have great potential for the creation of novel pumps, motors, and circuitry. Control of these devices requires an oscillator, either as a driver or clock circuit, which is typically provided as part of bulky, rigid, and costly external electronics. Oscillator circuits based on piezo-resistive dielectric elastomer switch technology provide a way to embed oscillatory behavior into artificial muscle devices. Previous oscillator circuits were not digital, able to function without a spring mass system, able to self-start, or suitable for miniaturization. In this paper we present an artificial muscle ring oscillator that meets these needs. The oscillator can self-start, create a stable 1 Hz square wave output, and continue to function despite degradation of the switching elements. Additionally, the oscillator provides a platform against which the performance of different dielectric elastomer switch materials can be benchmarked.**

***Index Terms*—Artificial muscle, dielectric elastomer, ring oscillator, switch.**

I. Introduction

Dielectric elastomer artificial muscles are a new class of soft, flexible actuator [1], [2] with great potential for a wide range of applications including motors, peristaltic pumps, conveyors, vibrotactile displays, and inchworm or rolling robots [3]–[8]. These devices all have an oscillatory element to their control, typically provided as part of an external suite of sensor, driver, and control circuitry. This circuitry is not soft or lightweight, as can be seen in the literature [9], [10], and it would be ideal if oscillators could be directly embedded into artificial muscle devices instead.

Recently, we presented Dielectric Elastomer Switch(es) (DES)—strongly piezoresistive elements that, when deformed, can directly

Manuscript received March 16, 2011; revised June 16, 2011; accepted August 14, 2011. Date of publication September 19, 2011; date of current version January 9, 2012. Recommended by Technical Editor R. B. Mrad. This work was supported in part by the Royal Society of New Zealand with a Rutherford Foundation Postdoctoral Fellowship awarded to B.M. O'Brien.

B. M. O'Brien is with the Biomimetics Laboratory, Auckland Bioengineering Institute, University of Auckland, Auckland 1010, New Zealand, and also with the Microsystems for Space Technologies Laboratory, EPFL, CH-2002 Neuchâtel, Switzerland (e-mail: ben.obrien@auckland.ac.nz).

I. A. Anderson is with the Biomimetics Laboratory, Auckland Bioengineering Institute, University of Auckland, Auckland 1010, New Zealand, and also with the Department of Engineering Science, Faculty of Engineering, University of Auckland 1010, New Zealand (e-mail: i.anderson@auckland.ac.nz).

Digital Object Identifier 10.1109/TMECH.2011.2165553

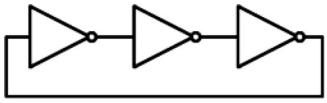

Fig. 1. Simple three-stage ring oscillator. As the number of inverters is odd the ring is unstable and will oscillate as fast as the components allow.

switch the high voltages required for Dielectric Elastomer Actuator(s) (DEA)—allowing for the creation of complex electromechanical circuits [11]. In the same paper, we demonstrated that a network of DES and DEA could be used to create an analogue oscillator. The analogue oscillator showed promise as a clock or driver circuit, however it had some key limitations. Specifically it was not: 1) digital, allowing for tolerance to degradation and fabrication variability; 2) based solely on DES/DEA interaction, allowing for oscillation without a mass-spring system; 3) suitable for miniaturization, required for the creation of faster artificial muscle circuitry; or 4) able to self-start.

In the present paper, we propose that ring oscillator architectures meet these requirements. Ring oscillators are formed by an odd number of digital inverters connected into a ring, as shown in Fig. 1 [12]. Because of the uneven number of inverters the feedback from the final stage inverts the input to the first stage. This configuration is unstable and oscillates as fast as the inverters allow. Ring oscillators are simple to make, can self-start, and are used in applications including clock recovery circuits, phase locked loops, crystal-free oscillators, multifrequency oscillators, random number generators, and process variability analysis [13]–[21].

In this paper, we present a novel artificial muscle ring oscillator that is digital, based on DES/DEA interaction, can self-start, is suitable for miniaturization, and provides a benchmarking tool for the analysis of new DES materials and fabrication techniques. Development of the three-stage oscillator is presented first, followed by results characterizing its start-up, stable oscillation, and degradation behavior. The discussion and conclusions focus on failure modes and a performance analysis of the device.

II. Materials and Methods

The oscillator was formed out of three inverters, and each inverter was formed out of two subunits, one of which is shown in Fig. 2. Each subunit consisted of a membrane that supported a two-part DEA (variable capacitor in the equivalent circuit) and a central DES (variable resistor). When the DEA actuated they relaxed the membrane, which compressed the switch and caused a substantial reduction in resistance due to an increase in the density of the electrode material. This interaction is represented with an arrow and minus sign to indicate that an increase in voltage on the DEA results in a decrease in resistance of the DES.

The membrane was formed by prestretching VHB 4905 equibiaxially to 12.25 times its original area and adhering it to a 75 mm inner diameter perspex ring. The DEA electrodes were made of Nyogel 756G and the two halves of the DEA were connected electrically in parallel. The DES electrodes were made of a 5:1 by weight mix of Molykote 44 medium grease and Cabot Vulcan XC72 carbon black applied with a size 0 taper point soft color shaper from Royal Sovereign Ltd. U.K., as presented in [11]. The DES were also in two parts as can be seen in the schematic of Fig. 2; the horizontal grey stripes were applied during prestretching so that they were 35% stretched, and thus highly nonconductive at rest; the black lines were unstretched and always conductive interconnects.

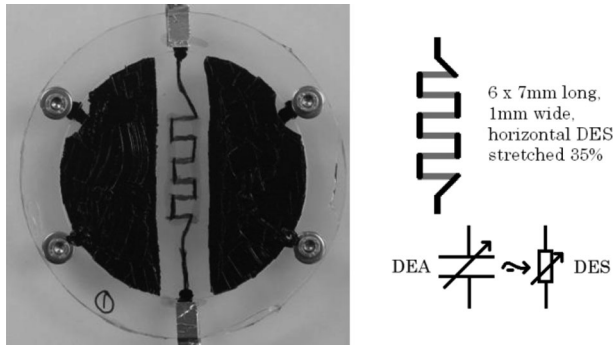

Fig. 2. Oscillator subunit. An equivalent circuit is given where the two DEA are lumped into one variable capacitor and the DES is represented by a variable resistor. When activated, the DEA compresses the DES, lowering its resistance as represented by the negative sign on the arrow. The switching sections of the DES are horizontal; the vertical sections are interconnects.

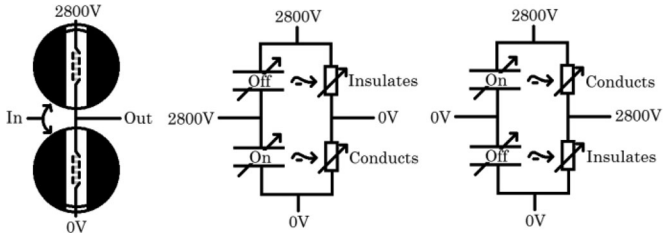

Fig. 3. Inverter schematic and equivalent circuit. Two subunits were connected (left) so that the output would be low when the input was high (middle), and the output high when the input was low (right).

Fig. 4. Ring oscillator during oscillation. Three inverters are connected in a ring (bottom → middle → top) and when powered will oscillate.

Fig. 3 shows how the subunits were arranged in pairs to form inverters. One subunit in each inverter was referenced against the 2800 V supply, and the other subunit was referenced against 0 V. Considering the left circuit of Fig. 3, it can be seen that with a 2800 V input the output will be close to 0 V. Considering the right circuit of Fig. 3, it can be seen that with a 0 V input, the output will be close to 2800 V.

Three inverters were connected into a ring (refer Fig. 1) to form the oscillator. A still image from the fabricated oscillator undergoing oscillation is given in Fig. 4. In this image, the inverters are connected in the order bottom → middle → top. The oscillator was powered from a 4-channel EAP control unit at 2800 V (Biomimetics Lab, Auckland

TABLE I
RING OSCILLATOR PERFORMANCE SUMMARY

Performance Metric	Value
cycles until failure	~140
frequency of operation	~1 Hz
average delay per inverter	~0.17 s
amplitude (peak to peak)	100% of supply (2800 V)
waveform	~square

NZ). To provide enough current, a WYE configuration of 15 kOhm resistors was used to tie three 125 μA power supply channels together.

To help understand the oscillator, we can ignore delays and represent the action of each inverter recursively using

$$V_{n+1} = -K\left(V_n - \frac{1}{2}V_H\right) + \frac{1}{2}V_H \tag{1}$$

where V_H is the high voltage supply, currently 2800 V, V_{n+1} is the output voltage of the inverter and must be between V_H and ground, V_n is the output voltage of the previous inverter, and the input to the present inverter, and *K* is the gain of the inverter.

Consider all the outputs initially sitting at half V_H. Equation (1) predicts that with an input voltage of half V_H the inverters will output the same and no oscillations will occur. But it is more likely that manufacturing imperfections will cause the outputs to be slightly different to the inputs. Then consider that if the first inverter were to output higher than half V_H to the second, the second would output lower than half to the third, and the third would output higher than half to the first, and so on. Oscillations would build up until the inverters were saturated and the ring oscillator stabilized. It can be seen that the gain *K* must be greater than 1, or else oscillations will decay to zero, and ideally as large as possible, to make the device better at self-starting.

III. RESULTS

The supply was switched ON and the oscillator ran until it failed due to degradation. The output was connected to a 5 GOhm input impedance voltage probe and data were acquired using a National Instruments DAQ card and Labview 2009. Table I summarizes the performance of the oscillator, where the average delay per inverter was calculated as the period of the oscillator divided by 6, which is the total number of inverter transitions per oscillation period (see McNeill and Ricketts, p. 21, Eq. 2.1 [12]). Fig. 5 shows the first 50 s of operation—note that the amplitude and frequency of the oscillator built up over time until it settled into a stable, saturated pattern. Fig. 6 shows the ring stably oscillating at a little more than 1 Hz, 100 s into the experiment. Fig. 7 shows the oscillator performance degrading due to spark erosion 170 s into the experiment, and the experiment was stopped at the 200 s mark before this degradation became fatal.

IV. DISCUSSION

The ring oscillator successfully self-started and formed a stable 1 Hz square wave oscillation as intended. This demonstrates that the loop gain was greater than one and that the switching delay of each inverter stage was approximately 0.17 s. As the supply voltage remained stable, we can say that the speed of the inverters was limited either by their RC time constants ($\tau = RC$, *where R is the DES ON-state resistance and C is the input capacitance of the next inverter*), the viscoelastic response of the VHB membrane, or time dependence of the switching compound. A study to establish what is limiting the speed could potentially be done by introducing resistance between the inverter stages, building the oscillator out of a less viscous membrane, and testing different materials for switching. It is anticipated that miniaturization of the device would allow it to run at greater frequencies as mechanical wave speed limits and RC time constants would be reduced. Further work could also include experiments to see how different supply voltages affect the oscillator behavior, and coupling the device to circuits or loads to be driven.

The oscillator had a limited life span, which was due to spark erosion on the DES elements. The erosion occurred at the interface between the stretched and unstretched switching material (grey and black lines in the Fig. 2 enlargement). The oscillator was repaired multiple times by

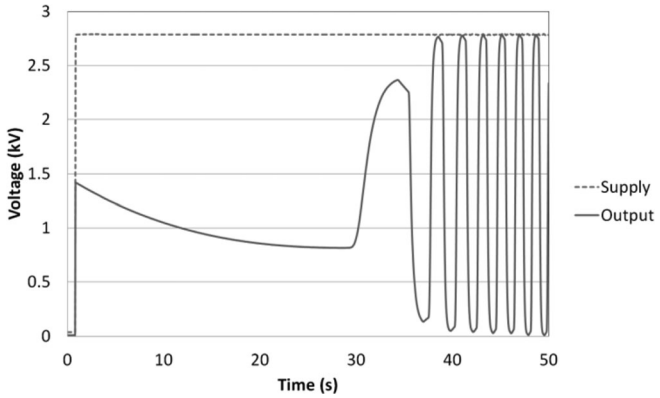

Fig. 5. Ring oscillator startup behavior. The amplitude and frequency grew until the ring settled into a stable oscillation.

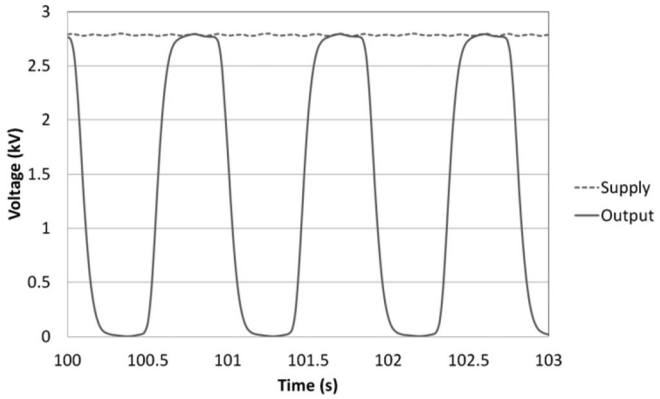

Fig. 6. Sample ~1 Hz stable oscillation 100 s into the experiment. Note that the power supply was steady and did not create the oscillation.

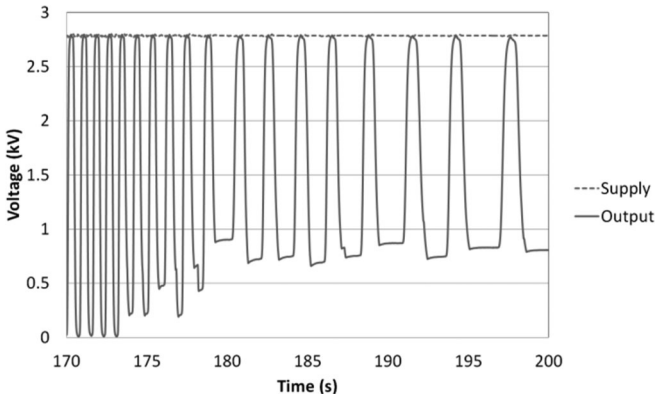

Fig. 7. Oscillator degradation. 170 s into the experiment the oscillation quality and speed began to degrade appreciably due to spark erosion.

painting over the ablated sections; it would then run until the erosion built up again. The data presented in this paper were after four such maintenance efforts. Several things could be done to reduce this erosion.

1) Reduce electric fields, possibly below some critical ablation threshold, by increasing DES track lengths.
2) Smooth the interface between DES and interconnects to eliminate electrical discontinuities.
3) Change the switching material to one less prone to ablation or use encapsulations for protection.
4) Use DEA that operate at lower voltages.
5) Conduct further experiments such as humidity, temperature, and pressure tests to better understand the ablation process.

It is worth pointing out the inherent tolerance of the oscillator to this ablation. The ring exhibited regular, clean oscillations until degradation built up to some threshold, and even then it was still able to function in a reduced capacity. This tolerance is possibly due to the digital nature of the oscillator. The likely effect of DES ablation is to shift or change the shape of the compression/conductivity curve so that a larger compression is required to make the switch conduct. This has no effect on a digital system as long as the threshold lies between the ON and OFF states. Analogue systems are much more susceptible as their operation point lies on the transition itself.

The ring oscillator is particularly well suited to driver applications such as multiphase motors or pumps as each inverter stage can act as an out-of-phase output. For acting as a clock for artificial muscle digital circuitry, the oscillator does not require a discrete spring mass system and thus should exhibit lower susceptibility to environmental vibrations, and should be easier to miniaturize. Ring oscillators enjoy a long history of being used as test-beds for new hardware, and an artificial muscle oscillator is no exception. The oscillator presented here provides a test system against which new switching materials can be tested. Candidate materials could include ion-implanted metals, metal films, and a wide range of carbon or silver-loaded silicones and greases [22]–[24]. In addition to exploring electrodes, new membrane materials such as silicone may improve reliability, speed and efficiency of the device. We propose that the future development of these materials and their associated fabrication techniques should be benchmarked using ring oscillators and against the data presented in Table I.

V. Conclusion

We have presented an artificial muscle ring oscillator built out of a network of coupled DEA and DES elements. The ring oscillator self-started and ran stably at approximately 1 Hz for 140 s before degrading due to spark erosion. The oscillator has the critical advantages that it does not rely on coupled mass-spring system, it should be easy to miniaturize, and it provides a standardized test against which future developments can be compared. The oscillator will be especially well suited to multiphase pump and motor driver circuitry, once degradation issues have been addressed.

Acknowledgment

The authors thank the Auckland Bioengineering Institute and the University of Auckland, everyone in the Biomimetics Laboratory, especially T. A. Gisby, T. G. McKay, H. C. Lo, and S. H. Walbran, friends and family, M. W. O'Brien, M. J. O'Brien, and M. C. O'Brien.

References

[1] R. E. Pelrine, R. D. Kornbluh, Q. Pei, and J. P. Joseph, "High-speed electrically actuated elastomers with strain greater than 100%," *Science*, vol. 287, pp. 836–839, 2000.

[2] J. D. W. Madden, N. A. Vandesteeg, P. A. Anquetil, P. G. A. Madden, A. Takshi, R. Z. Pytel, S. R. Lafontaine, P. A. Wieringa, and I. W. Hunter, "Artificial muscle technology: Physical principles and naval prospects," *IEEE J. Oceanic Eng.*, vol. 29, no. 3, pp. 706–728, Jul. 2004.

[3] I. A. Anderson, T. Hale, T. Gisby, T. Inamura, T. McKay, B. O'Brien, S. Walbran, and E. P. Calius, "A thin membrane artificial muscle rotary motor," *Appl. Phys. A, Mater. Sci. Process.*, vol. 98, no. 1, pp. 75–83, 2010.

[4] F. Carpi, C. Menon, and D. De Rossi, "Electroactive elastomeric actuator for all-polymer linear peristaltic pumps," *IEEE/ASME Trans. Mechatronics*, vol. 15, no. 3, pp. 460–470, Jun. 2010.

[5] B. O'Brien, T. Gisby, S. Xie, E. Calius, and I. Anderson, "FEA of dielectric elastomer minimum energy structures as a tool for biomimetic design," in *Proc. SPIE*, San Diego, CA, 2009, vol. 7287, DOI: 10.1117/12.815818.

[6] K. Jung, J. C. Koo, J.-d. Nam, Y. K. Lee, and H. R. Choi, "Artificial annelid robot driven by soft actuators," *Bioinspir. Biomim.*, vol. 2, pp. S42–S49, 2007.

[7] P. Lotz, M. Matysek, and H. F. Schlaak, "Fabrication and application of miniaturized dielectric elastomer stack actuators," *IEEE/ASME Trans. Mechatronics*, vol. 16, no. 1, pp. 58–66, Feb. 2011.

[8] Artusi, M., M. Potz, J. Aristizabal, C. Menon, S. Cocuzza, and S. Debei, "Electroactive elastomeric actuators for the implementation of a deformable spherical rover," *IEEE/ASME Trans. Mechatronics*, vol. 16, no. 1, pp. 50–57, Feb. 2011.

[9] M. Babič, R. Vertechy, G. Berselli, J. Lenarčič, V. Parenti Castelli, and G. Vassura, "An electronic driver for improving the open and closed loop electro-mechanical response of dielectric elastomer actuators," *Mechatronics*, vol. 20, no. 2, pp. 201–212, 2010.

[10] J. Maas, C. Graf, and L. Eitzen, "Control concepts for dielectric elastomer actuators," in *Proc. SPIE*, San Diego, CA, 2011, vol. 7976, DOI: 10.1117/12.879938.

[11] B. M. O'Brien, E. P. Calius, T. Inamura, S. Q. Xie, and I. A. Anderson, "Dielectric elastomer switches for smart artificial muscles," *Appl. Phys. A: Mater. Sci. Process.*, vol. 100, no. 2, pp. 385–389, 2010.

[12] J. A. McNeill and D. S. Ricketts, *The Designer's Guide to Jitter in Ring Oscillators*, K. Kundert, Ed., New York: Springer, 2009.

[13] D. Liang and R. Harjani, "Design of low-phase-noise CMOS ring oscillators," *IEEE Trans Circuits Syst. II, Analog Digital Signal Process.*, vol. 49, no. 5, pp. 328–338, May 2002.

[14] G. Xiaoqing, M. Arcak, and K. N. Salama, "Nonlinear analysis of ring oscillator circuits," in *Proc. American Control Conf.,* 2010, Baltimore, MD, pp. 1772–1776.

[15] T. Nakura, M. Ikeda, and K. Asada, "Ring oscillator based random number generator utilizing wake-up time uncertainty," in *Proc. IEEE Asian Solid-State Circuits Conf.*, 2009, pp. 113–116.

[16] H. Le, B. Langley, J. Cottle, and T. E. Kopley, "Improved ring oscillator design techniques to generate realistic AC waveforms for reliability testing," in *Proc. 2000 IEEE Int. Integr. Reliability Workshop Final Report*, Lake Tahoe, CA, pp. 155–157.

[17] M. Z. Straayer and M. H. Perrott, "A multipath gated ring oscillator TDC with first-order noise shaping," *IEEE J. Solid-State Circuits*, vol. 44, no. 4, pp. 1089–1098, Apr. 2009.

[18] Nizhnik, O., R. K. Pokharel, H. Kanaya, and K. Yoshida, "Low noise wide tuning range quadrature ring oscillator for multistandard transceiver," *IEEE Microw. Wireless Compon. Lett.*, vol. 19, no. 7, pp. 470–472, Jul. 2009.

[19] B. Razavi, "A study of phase noise in CMOS oscillators," *IEEE J. Solid-State Circuits*, vol. 31, no. 3, pp. 331–343, Mar. 1996.

[20] B. Nikolic, B. Giraud, G. Zheng, L-T. Pang, J-H. Park, and S. O. Toh, "Technology variability from a design perspective," in *Proc. IEEE Custom Integr. Circuits Conf.*, Sep. 19–22, 2010, pp. 1–8.

[21] M. Farazian, P. S. Gudem, and L. E. Larson, "A CMOS multiphase injection-locked frequency divider for V-band operation," *IEEE Microw. Wireless Compon. Letters*, vol. 19, no. 4, pp. 239–241, Apr. 2009.

[22] F. Carpi, P. Chiarelli, A. Mazzoldi, and D. D. Rossi, "Electromechanical characterization of dielectric elastomer planar actuators: Comparative evaluation of different electrode materials and different counterloads," *Sensors Actuators A*, vol. 107, pp. 85–95, 2003.

[23] G. Kofod, P. Sommer-Larsen, C. Federico, R. Danilo De, K. Roy, P. Ronald, and S.-L. Peter, "Compliant electrodes: Solutions, materials, and technologies," in *Dielectric Elastomers as Electromechanical Transducers*. Amsterdam, The Netherlands: Elsevier, 2008, pp. 69–76.

[24] P. Dubois, S. Rosset, S. Koster, J. Stauffer, S. Mikhailov, M. Dadras, N.-F. deRooij, and H. Shea, "Microactuators based on ion implanted dielectric electroactive polymer (EAP) membranes," *Sensors Actuators A*, vol. 130–131, pp. 147–154, 2006.